High-contrast imaging results with the vortex coronagraph

E. Serabyn, J. Trauger, D. Moody, D. Mawet, K. Liewer, et al.

E. Serabyn, J. Trauger, D. Moody, D. Mawet, K. Liewer, J. Krist, B. Kern, "High-contrast imaging results with the vortex coronagraph," Proc. SPIE 8864, Techniques and Instrumentation for Detection of Exoplanets VI, 88640Y (26 September 2013); doi: 10.1117/12.2024660

SPIE.

Event: SPIE Optical Engineering + Applications, 2013, San Diego, California, United States

High-contrast imaging results with the vortex coronagraph

E. Serabyn*[a], J. Trauger[a], D. Moody[a], D. Mawet[b], K. Liewer[a], J. Krist[a], B. Kern[a]
[a]Jet Propulsion Laboratory, California Institute of Technology, 4800 Oak Grove Drive, Pasadena, CA, USA 91109; [b]European Southern Observatory, Alonso de Cordova 3107, Vitacura, Casilla 19001, Chile

ABSTRACT

The vortex coronagraph has already enabled high-contrast observations very close to bright stars on large ground-based telescopes, and it also has great potential for use on coronagraphic space missions aimed at exoplanet detection and characterization. As such, demonstrations of vortex coronagraph performance have recently been carried out in JPL's High Contrast Imaging Testbed. Some of our recent results are presented here, including the suppression of a monochromatic, single-polarization point-source to below the 10^{-9} level over a dark hole covering both the 2-7 λ/D and 3-8 λ/D regions, as well as the suppression of a 10% band of white-light to approximately the 10^{-8} level over a 3-8 λ/D dark hole.

Keywords: vortex optics, coronagraphy

1. INTRODUCTION

Experiments on the vortex coronagraph were carried out in the Jet Propulsion Laboratory's High Contrast Imaging Testbed[1] (HCIT) during two separate runs, in the autumn of 2012 and the spring of 2013. Some experimental results from these runs are briefly discussed here.

1.1 The HCIT

To demonstrate the deep suppression of a point source of light with any focal plane mask, the experimental facility must first be made capable of achieving the desired suppression level. Thus, much of our initial efforts were aimed at understanding the limitations of the facility, and modifying the system (e.g., Fig. 1) so as to enable measurements in the desired high-contrast regime. Several steps were crucial to reaching deep contrasts:

- Generation of a pure circularly-polarized input beam by installing a linear polarizer and quarter wave plate upstream of the existing "source pinhole," and by installing an in-line fiber polarization controller to tune the input fiber's output polarization state to match the free-space polarizer's vertical transmission axis.
- Investigation of contrast in the desired off-axis "dark hole" suppression region vs. the diameter of the pupil stop on the deformable mirror (DM). Best rejection was obtained for the smallest (24 mm) aperture stop used.
- Improved coupling of the HCIT input beam to the focal-plane vortex phase mask by means of improved pointing and focus procedures, and by reducing and also anticipating residual pointing drift.
- Improved spectral polarization filtering, aimed at broadening the suppression pass band for the selected polarization state, by means of an upgraded circular polarizer located downstream of the Lyot stop.
- Installation in the post-Lyot-stop focal plane of a "reverse-D"-shaped field stop only slightly oversized relative to the dark hole located there, in order to block most of the light outside of the dark hole from reaching the camera directly or scattering off of the optics downstream of the field stop.

Most of these individual steps yielded relatively modest performance improvements (typically less than about a factor of 2), but all of the steps together led to a significant improvement over our earlier results[2,3].

*gene.serabyn@jpl.nasa.gov; phone 1 818 640-7485; fax 1 818 393-4357

Techniques and Instrumentation for Detection of Exoplanets VI, edited by Stuart Shaklan, Proc. of SPIE Vol. 8864, 88640Y · © 2013 SPIE · CCC code: 0277-786X/13/$18 · doi: 10.1117/12.2024660

All of our final tests were thus carried out (Fig. 1) with vertically polarized input light that was converted to a circular polarization state by means of a quarter wave plate oriented at 45° to the vertical, prior to passage through a 5 micron "source" pinhole. A clear beam diameter, D, of 24 mm was then defined at the DM, and after passage through the focal plane vortex phase mask and the subsequent clear pupil-plane Lyot stop (with a size 83% of the pupil diameter), a downstream circular polarizer (a quarter wave plate followed by a linear polarizer) was used to select the high-contrast polarization state. Finally, most of the non-essential light beyond the dark hole was eliminated by the field stop.

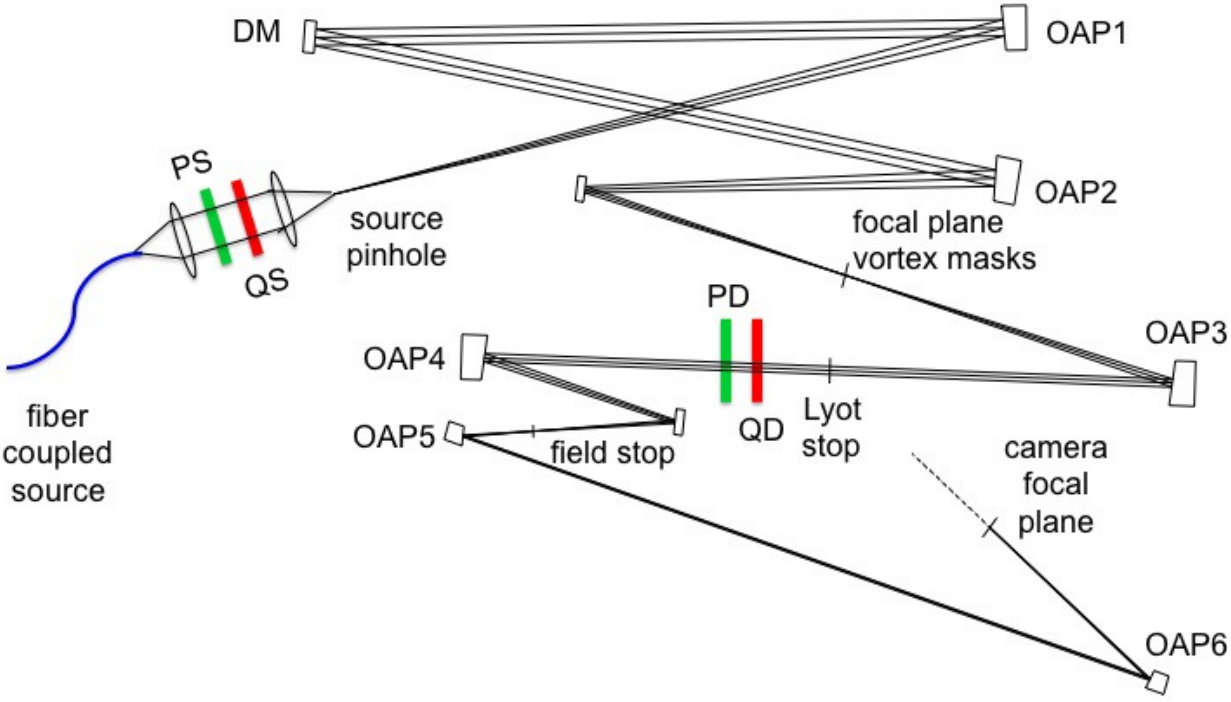

Figure 1. Schematic of the HCIT optical layout, as used for our 2012/2013 tests of the vortex coronagraph. The input light is first circularly polarized with the combination of a fiber polarization controller (not shown) and a free-space "source" polarizer (PS) and quarter wave plate (QS). The light is then spatially filtered by means of a pinhole approximately 5 μn in diameter. The light is then collimated by the first off-axis paraboloid (OAP), reflects off of the deformable mirror (DM), where the circular aperture stop resides, and is focused onto the vortex phase mask (which resides on a coarse/fine positioning stage). The light is then recollimated for passage through a clear Lyot stop and a downstream quarter wave plate (QD) and polarizer (PD). Finally, the light is focused onto a reverse-D-shaped field stop that is slightly oversized relative to the desired dark hole, and relayed to the camera.

1.2 The vortex mask

Several vortex masks were tested during our HCIT runs, but the highest contrast dark holes were obtained with a "2nd generation" liquid-crystal-polymer 4th-order vector-vortex mask that was manufactured by JDS Uniphase and delivered in Oct. 2009. This mask is the same one as that tested during our brief foray into the HCIT in the spring of 2011. Due to manufacturing limitations at the time, this mask has a small central defect in the vortex pattern that has been covered with a 40 micron diameter opaque circular mask (Fig. 2). The mask was designed to meet the necessary half-wave condition at a wavelength of approximately 800 nm.

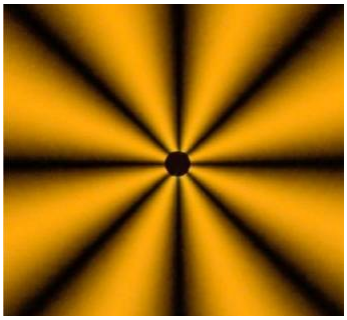

Figure 2. An image of the JDSU charge 4 liquid-crystal-polymer vector-vortex phase mask that was used in the HCIT tests described here. For the image, the vortex is between crossed polarizers.

2. PERFORMANCE RESULTS

2.1 Monochromatic Light

Contrast tests in monochromatic light were first carried out with a laser diode source at a wavelength, λ, of 785 nm. A subset of our results are shown in Figs. 3-5. Near the right-hand edge, Fig. 3 shows a schematic of the size and location of the targeted 3-8 λ/D dark hole region relative to the center of the point spread function (red star). Fig. 3 also shows the final images for each of three coronagraphic nulling sequences (in color), and the size and location of the 3-8 λ/D dark hole on the same image scale (bottom right). The outer edge of the bright "reverse D"-shaped region seen in the images corresponds to the field stop's inner edge, and the dark hole is the dim region inside the bright reverse D. These three nulling runs each began (on different days) by re-flattening the DM, so each run represents an independent wavefront control solution for the dark hole. Each of the three nulling runs reached similar average dark-hole suppression levels. Specifically, the average suppression levels in these three dark holes are 4.1 x 10^{-10}, 5.4 x 10^{-10}, and 5.2 x 10^{-10}.

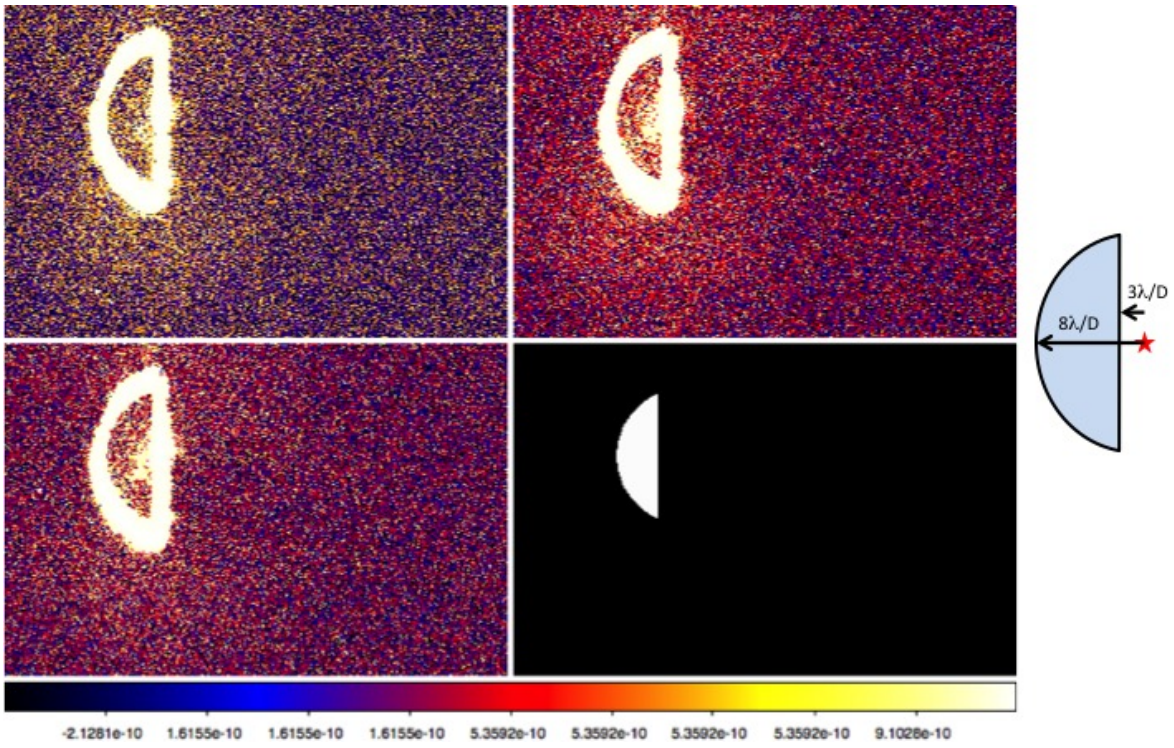

Figure 3. Right-hand edge: Schematic of the size and location of the targeted 3-8 λ/D dark hole relative to the location of the point source (red star) in the image plane. Colored panels: three images showing the final dark holes obtained at the end of three independent nulling runs. Bottom right: the size and location of the 3-8 λ/D dark hole on the same spatial scale.

Note that a slight excess of light (compared to the darker region at the right hand edge of the detector array) is present in the immediate vicinity of the reverse D, both inside and outside of it. The residual light within the dark hole represents the dark hole suppression level reached. The dim light beyond the reverse D, where none should be in the geometric optics case, implies some scattering or diffraction downstream of the field stop.

Fig. 4 shows dark hole results for a subsequent nulling run in which the targeted dark hole was shifted closer to the point source, specifically to 2-7 λ/D. A similar dark-hole average suppression of 5.1 x 10^{-10} was reached in this case. Finally, Fig. 5 compares radial contrast data from a pair of our 3-8 λ/D and 2-7 λ/D runs. The agreement between the two curves is quite close in the overlapping 3-7 λ/D region, and the suppression is below the 10^{-9} level everywhere but in the innermost 2-3 λ/D region, where it is 1.7 x 10^{-9}.

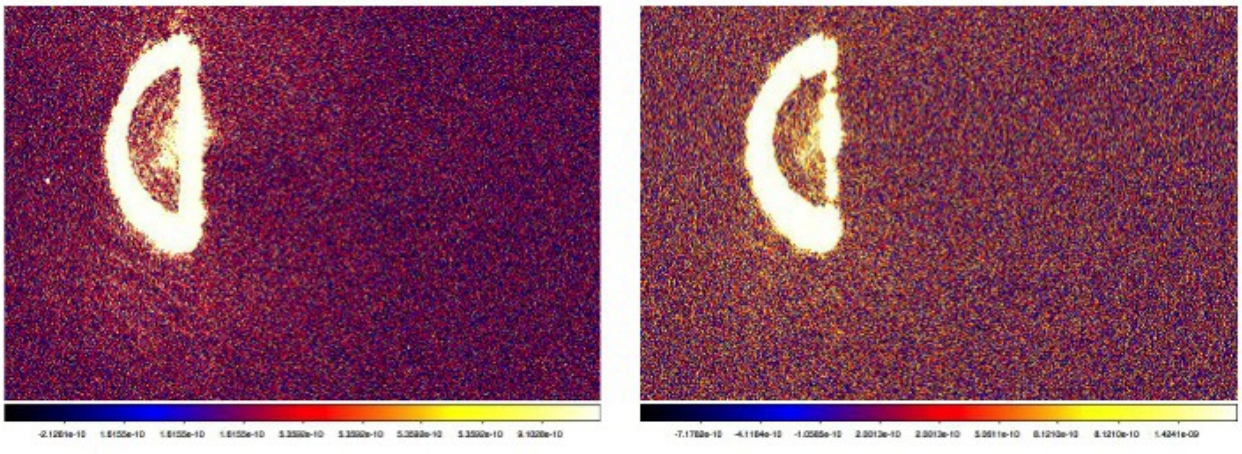

Figure 4. Shifting the dark hole inward toward the point source, i.e., from 3-8 λ/D in earlier runs (left panel) to 2-7 λ/D in later runs (right panel).

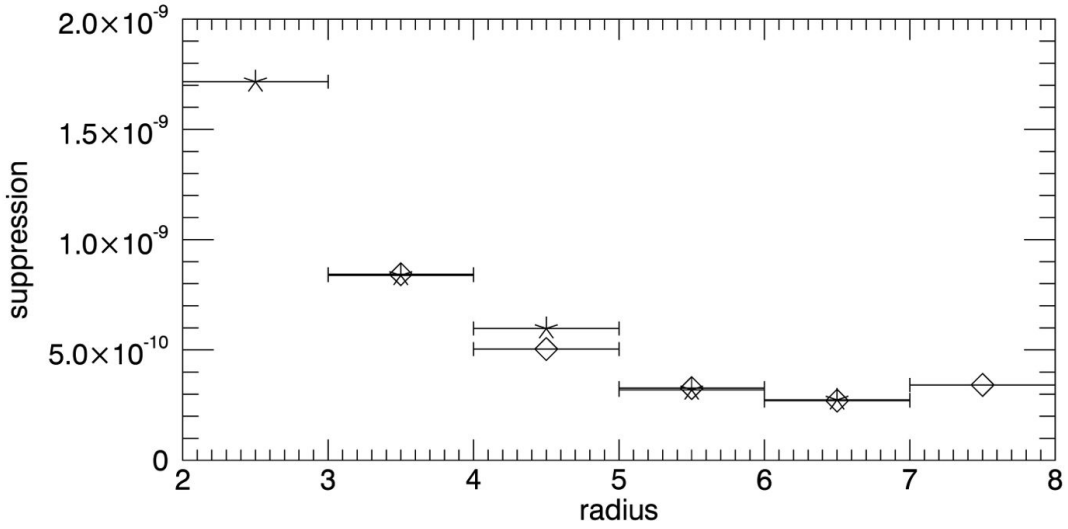

Figure 5. Superposition of radial contrast data obtained for two separate nulling runs that targeted dark holes covering 3-8 λ/D (diamonds) and 2-7 λ/D (asterisks). Each point shown is the average of the suppression data over radial intervals 1 λ/D wide. The two data sets overlay remarkably well in the 3-7 λ/D overlap region, and show a relatively small (factor of a few) brightness increase toward smaller radial offsets from the location of the light source.

2.2 Broadband Light

Tests with light covering a broader band were next carried out using a supercontinuum laser source and a series of five adjacent 2%-bandwidth spectral filters that together span a net bandwidth of 10%. The wavefront was optimized after sequentially carrying out wavefront sensing in all five bands. The resultant suppression is best at band center, and degrades towards the edges of the band. Except for a single persistent bright speckle that seems to be due to a small defect or dust particle, the 3-8 λ/D dark hole reached deep levels, with the average suppression over the full dark hole region in the full 10% band being 1.1 x 10^{-8}. Excluding the region of this single bright speckle, or, alternatively, averaging the suppression over only the top half of the dark hole, yields an average suppression in the remaining dark hole regions of 5.0 x 10^{-9} and 4.6 x 10^{-9}, respectively.

As a rotation of this focal plane mask could in principle remove the bright speckle from the dark hole region, the same vortex mask may be capable of yet deeper broadband suppression over a complete dark hole region. On the other hand, improved masks should also help broadband performance, and these should be available relatively soon.

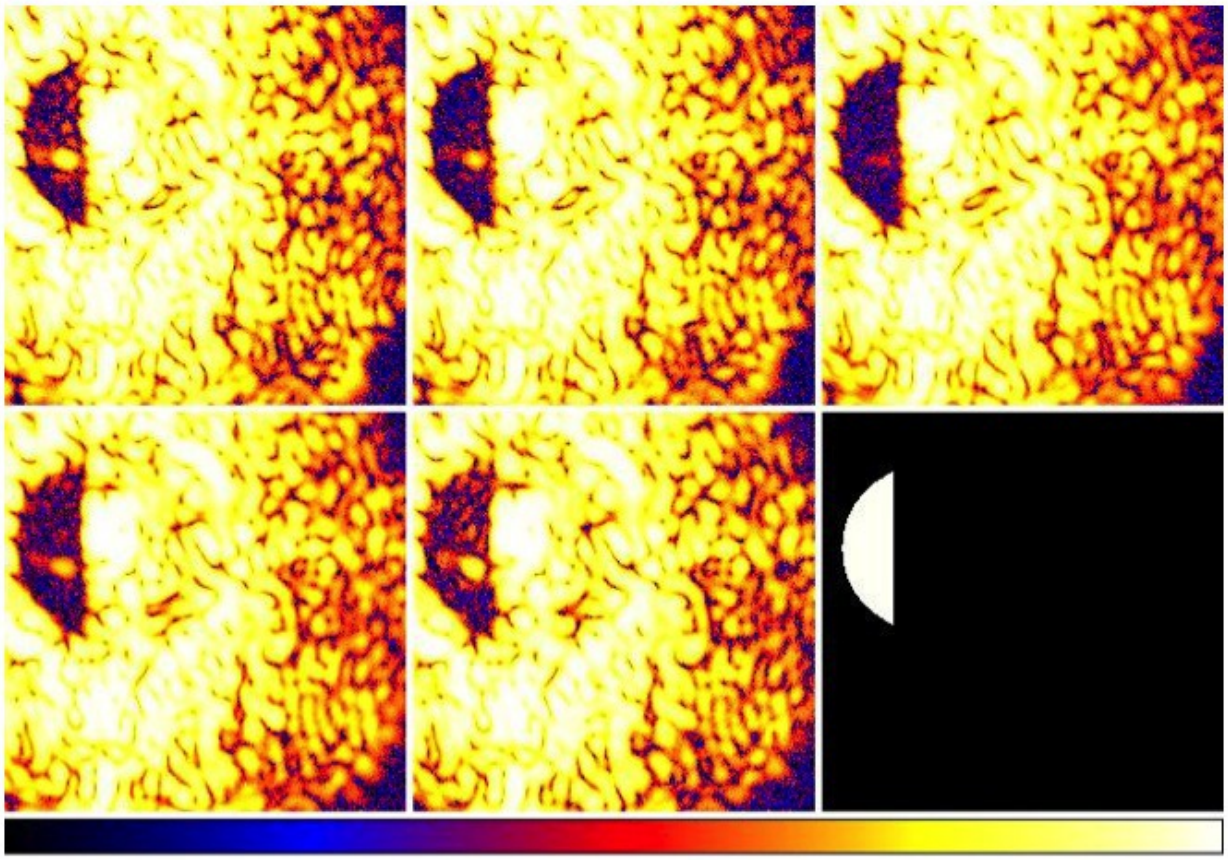

Figure 6. Color images: suppression of broadband incoherent light from a supercontinuum source in five adjacent 2%-wide bands. The five 2% passbands are centered at 768, 784, 800, 816, and 832 nm (right to left, top to bottom). For these images, no field stop was in place, so the entire point spread function is seen. The point spread function is centered on the bright spot just to the right of the dark hole. The suppression is best at band center, and degrades with wavelength offset. Lower right: the location of the targeted 3-8 λ/D dark hole on the same image scale.

This work was carried out at the Jet Propulsion Laboratory, California Institute of Technology, under contract with the National Aeronautics and Space Administration.

REFERENCES

[1] Trauger, J. T. and Traub, W. A., "A laboratory demonstration of the capability to image an Earth-like extrasolar planet," Nature 446 , 771–773 (2007).

[2] Mawet, D., Serabyn, E. Moody, D. Kern, Niessner, A., Kuhnert, A., Shemo, D., Chipman, R. McClain, S. and Trauger, J., "Recent results of the second generation of vector vortex coronagraphs on the high-contrast imaging testbed at JPL," Proc. SPIE 8151, 81511D-1-81511D-8 (2011).

[3] Serabyn, E. Mawet, D., Wallace, J.K., Liewer, K., Trauger, J., Moody, D., and Kern, B., "Recent Progress in Vector Vortex Coronagraphy," Proc. SPIE 8146, 81460L-1-81460L-8 (2011).